buildings

MDPI

Article

Regression Models for the Description of the Behaviour of Modern Timber Joints

Dorotea Caprio * and Robert Jockwer

Construction Technology, Chalmers University of Technology, 412 96 Gothenburg, Sweden; robert.jockwer@chalmers.se
* Correspondence: dorotea.caprio@chalmers.se

Abstract: Joints in timber structures are today typically designed in a simplistic manner, i.e., by assuming linear elastic behaviour or neglecting their real stiffness by assuming ideal pinned or fixed conditions. While such assumptions may be acceptable for simple structures, they do not reflect the real behaviour of joints in complex structures, and could, in some cases, lead either to an over-conservative or even unsafe design. Therefore, a more accurate and realistic representation of the nonlinear behaviour of joints with mechanical fasteners is needed. The most common modern timber joints with mechanical fasteners are realized with dowels, bolts, glued-in rods, or self-tapping screws. In this paper, an overview of the impact of the most influential parameters on the shape of the load-displacement curves of these joints under common static loading is given. The joints were differentiated according to the characteristics of their nonlinear load-displacement behaviour. Different analytical models from the literature for the description of the load-displacement curves of timber joints were reviewed. The performance and suitability of these models for describing the variety of nonlinear load-displacement behaviours of joints were evaluated and the advantages and limitations of each model were identified. It was found that the Richard–Abbott model is the most suitable to parametrize a variety of timber joints and to capture the variability of the test data by its parameters. Such an analytical model can be used to incorporate a parametrized, more realistic, nonlinear load-displacement representation of the behaviour of joints in reliability analyses, structural design software, and design guidance for modern timber structures.

Keywords: joint; connection; slip; slip-modulus; stiffness; ductility; wood; timber; regression models

Citation: Caprio, D.; Jockwer, R. Regression Models for the Description of the Behaviour of Modern Timber Joints. *Buildings* **2023**, *13*, 2693. https://doi.org/10.3390/buildings13112693

Academic Editor: Andreas Ringhofer

Received: 30 September 2023
Revised: 19 October 2023
Accepted: 20 October 2023
Published: 25 October 2023

1. Introduction

The performance of timber structures in terms of their load-carrying capacity, reliability, costs, vibration, robustness, etc., depends to a considerable extent on the behaviour of the joints. (The terms 'joint' and 'connection' are often used as synonyms in the literature. In [1], a connection is defined as the union of two or more joints and a joint is defined as an ensemble of fasteners with two or more members. In this paper, for the sake of clarity for the reader, the term "joint" is used also to indicate a connection between the different structural timber members [2]). Timber joints with mechanical fasteners display, in general, complex nonlinear behaviour, often with a variety of possible failure modes. Although experienced engineers will be aware of the need to represent the mechanical behaviour of joints in a more realistic, complex manner, for the sake of ease of use in design, and due to the lack of more detailed knowledge, the behaviour and properties of the joints are often simplified. For example, when designing timber structures, joints with mechanical fasteners are usually regarded as either pinned or clamped, while their real behaviour is closer to that of semi-rigid joints [3]. Furthermore, the load-displacement behaviour of these joints is considered to be linear-elastic, whereas in reality, it might be highly nonlinear.

The relevance of joints and their impact on timber structures is particularly important when dealing with modern and complex timber structures, such as large-span structures,

tall timber buildings, and statically indeterminate timber structures [4,5]. These modern timber structures are typically made from engineered wood products, such as glued-laminated timber (glulam), laminated veneer lumber (LVL), or cross-laminated timber (CLT). The importance of proper design and consideration of joints is highlighted by the fact that the improper design and manufacturing of joints is the main cause of the collapse of modern timber structures [6].

In general, the established properties for the description of the nonlinear load-displacement behaviour and structural performance of joints are the elastic stiffness, the load-carrying capacity, and the displacement capacity (or ductility). However, traditionally, and in some cases also nowadays, the methodology to design timber structures is based on a components check, where only the load-carrying capacity of the members and joints are accounted for, whereas the displacement capacity is often disregarded [7] and a more detailed push-over analysis is not carried out for static cases. Also, in design codes, such as Eurocode 5 (EC5) [8], the load-carrying capacity of timber joints is the most detailed aspect. The EC5 code proposes the so-called European yield model (EYM) for calculating the load-carrying capacity of laterally loaded dowel-type fasteners whereas the models for the elastic stiffness are purely empirical and described based on the timber density and fastener diameter [9]. The suitability of the current design rules for elastic stiffness is often debated regarding the inability to capture the influence of additional important influencing parameters [9]. To account for the nonlinear load-displacement of joints in the ultimate limit state (ULS), the stiffness in the serviceability limit state (SLS) (elastic stiffness) is simply reduced by two-thirds. This is based on old models derived from test data on nailed joints in Australian timber from the 1960s [10]. The responsible engineer is left without guidance but a general statement that "the model for the calculation of internal forces in the structure… shall take into account the effects of displacements of the connections". In addition, no statements about the displacement capacity (or ductility) of these joints are given in EC5. In research studies, large experimental campaigns of different types of timber joints have been conducted in an attempt to obtain detailed knowledge of their behaviour and load-carrying capacity. In this respect, the effects of the varying geometrical and mechanical parameters have also been studied. Much less detailed studies and experiments have been carried out on the elastic stiffness and ductility of timber joints, despite the fact that these two properties are highly relevant for the distribution of forces and the failure modes of statically indeterminate structures. Due to the natural variability in the material properties of timber, the consideration of uncertainties associated with the parameters describing the mechanical behaviour of joints (i.e., stiffness, load-carrying capacity, and ductility) is an important prerequisite to design reliable structures. The joint ductility is accounted for in the seismic design through ductility classes contained in Eurocode 8 (EC8) [11]. However, the elastic stiffness and ductility and their variability have an important impact on the reliability of statically indeterminate structures at static ULS as well, thus not only under seismic or exceptional actions alone [2,12].

A variety of analytical models and equations for the description of the nonlinear load-displacement behaviour of joints have been proposed by previous researchers [13–17]. The equations derived are based on, e.g., exponential functions, power functions, a combination of the two, polynomials, and rational functions.

Analytical models can be used directly as input for the realistic description of the nonlinear behaviour of joints for the structural analysis or they can be parametrized to describe the behaviour depending on other parameters (load-to-grain angle, density, load-to-fasteners, etc.).

In [18], a multi-step approach for the parametrization by means of the Richard–Abbott regression function was applied to describe the embedment behaviour of a single dowel as a function of the wood orthotropy. This function was used in a later publication as input for a semi-analytical model of a multi-dowel moment resisting joint [19]. In [20], a parametrized description for multi-dowel timber joints was developed with slotted-in plates as the input for a reliability analysis of timber trusses. In [16], a description of the

load-displacement behaviour of hold-down and angle bracket joints was used as input for the prediction of the lateral load-displacement behaviour of a CLT wall system.

Although these studies were a first attempt at a more precise description of the nonlinear behaviour of joints, they do not cover the large variety of modern timber joints that exist in practice, such as joints with glued-in rods (GiR) and joints with self-tapping screws (STS). Therefore, consideration of the suitability of analytical models and their ability to approximate the diverse load-displacement behaviour of a larger variety of timber joints is needed. Parametrized models of the nonlinear load-displacement behaviour of modern timber joints and the variability of the model parameters are also needed to perform reliability analyses of modern and complex timber structures.

In this study, first, an overview of the diverse shapes of the load-displacement curves of the most common timber joints was undertaken. Joints with dowels and bolts, joints with GiR and joints with STS were covered. Previously proposed analytical models were reviewed and applied to a selection of relevant load-displacement curves, and subsequently, their regression performance and suitability were evaluated and discussed. The work is limited to the description of the force (load)-displacement behaviour of timber joints. However, although not addressed in this paper, in order to accurately describe certain types of joints, a description of moment-rotation behaviour might be required. This work enables engineers to incorporate a more realistic description of timber joints in structural analyses. The analytical models of timber joints can be parametrized as a function of the most influential parameters and used as input for the representation of timber joints as nonlinear springs in the structural analysis and reliability analysis of structures.

2. Overview of Joint Behaviour in Timber Structures

2.1. General

A large variety of joint typologies and technologies exist for modern timber structures; in the case of high performance requirements, the majority of joints are effected by dowels, including GiR or STS.

Joints with laterally loaded metal dowels are, for example, used in combination with slotted-in or outer steel plates in trusses [4], medium- to high-rise buildings [5], and in bridges [21]. In the design, the rotational stiffness of closely spaced small groups of dowels is often neglected even if they are subjected to moment action due to eccentricities [20]. Larger groups of dowels and groups with larger spacing between the dowels can be employed as moment-resisting joints, e.g., in frame corners, where the dowels are positioned at a distance around the center of rotation [22].

GiR rely on the bond between the timber and (steel) rod by means of adhesive, which provides a degree of slipness but brittle joints through the bondline. Therefore, GiR are well suited for applications requiring high stiffness. GiR can be used to couple a steel member with a timber member or to join two timber elements. Joints with GiR are often used to realize moment-resisting joints, such as beam-to-column or beam-to-beam joints, with or without steel profiles [22] or column foundation [23]. Ductile behaviour can be archived under monotonic and cyclic loading if the relevant failure is the yielding of the steel and not the failure modes associated with the timber. GiR are also used for the reinforcement and repair of timber members [24].

Axially loaded STS provide high resistance and stiffness; therefore, shear joints with inclined STS are used for high-performance joints, e.g., in moment-resisting joints in domes [4] and grid-shells [25], or in large structures, such as arches as interior joints to restore the continuity of the arch [26], and in beam-column joints [4]. Ductile behaviour of STS joints can be obtained if the screws are mostly laterally loaded or if the screws are placed in a combined arrangement, i.e., inclined and perpendicular to the shear plane [27].

STS represent the state-of-art joining technique in CLT-based structures [27]. In fact, STS are used in CLT-based structures, i.e., to realize butt joints, half-lap joints or spine joints. STS can also be used, if inclined, to connect two orthogonally positioned CLT walls [28], or, if coupled with steel plates, as angle brackets and hold-downs in wall-to-floor and

wall-to-wall joints [16]. Fully threaded STS are also frequently applied as reinforcement against stresses in the weak directions of timber members, e.g., as reinforcement in laterally loaded dowel-type joints [29].

Laterally loaded dowels and bolts are very frequently used in joints, due to their good performance [30]; they possess moderate load-carrying capacity and, when well-designed, considerable ductility. In addition, they are cheap and easy to install. GiR in joints are most often subjected to pure axial tension or predominant axial tension and minor lateral forces, while STS in joints are often subjected to a combination of lateral and axial forces, especially when STS are inclined with respect to the shear plane. For this reason, in the following subsections, the parameters of influence on the load-displacement behaviour of joints with laterally loaded metal dowels loaded laterally, GiR loaded axially, and STS loaded in combined shear and axial loading are analyzed.

The shape of the load-displacement curves changes according to the typology of the joints, i.e., depending on the type, the configuration (e.g., spacing, edge distances, number of rows) of the fasteners, and the failure mode of the joint. However, the load-displacement of all joints broadly shows three distinct regions (see Figure 1) [31]:

- A region of low or "zero stiffness", at very low load levels, usually due to delayed contact between parts [31,32].
- An elastic region, characterized by a quasi-proportional relationship between the displacement and the load [31].
- A plastic region [31] that can further develop with a softening branch, with a plateau, or with a hardening branch. A hardening branch may occur due to the so-called rope effect in laterally loaded fasteners, which is caused, among other things, by normal forces in the fasteners and friction in the shear plane [33].

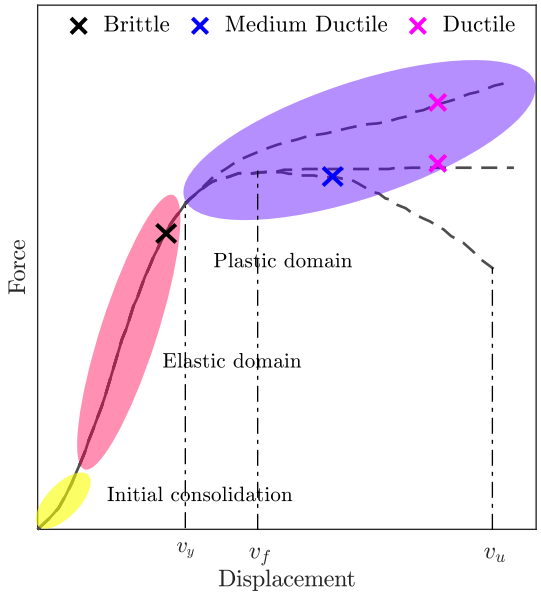

Figure 1. General description of load-displacement curve for timber joints. A similar figure can be found in [31].

The failure point can be located in the elastic or the plastic region. In the event it is in the elastic region, the failure is brittle due to the fracture of the wood or the steel rupture (e.g., if the fastener is also axially loaded) before major ductile mechanisms can take place [34]. When the failure point is situated in the plastic region, the failure can be described as moderately ductile or ductile. In the event that the plastic region has limited extension, the failure is typically due to the fracture of the wood after some yielding of fasteners has occurred or because of an early rupture of the fasteners (moderately ductile failure). The more the plastic region is extended, the more ductile the behaviour of the

entire joint (ductile failure). Final failure is reached when the displacement capacities of either the fastener or the timber are exceeded. In experiments and for classification, failure is often defined as the state when the load falls below a certain level in the softening branch or when a deformation criterion is reached.

Ductility is a desirable characteristic in timber joints since it benefits the robustness, reliability, and seismic performance of the structures [2,12,35]. For example, in statically indeterminate structures, the joints can behave as a source of ductility and energy dissipation, so the rotational ductility is a very important characteristic to be determined [35]. A review of the relative and the absolute definitions of ductility is given in [35–37]. The majority of definitions are displacement-based and they are written as a function of the displacement at the yielding point v_y and of the ultimate displacement (maximum load F_u) v_u or of displacement at failure v_f (after the maximum load F_u has occurred) (Figure 1). These two points are illustrated in Figure 1. The most common relative definitions are the following [35–37]:

$$D_{r,f} = \frac{v_f}{v_y} \tag{1}$$

$$D_{r,u} = \frac{v_u}{v_y}. \tag{2}$$

And the corresponding absolute definitions are:

$$D_{a,f} = v_f - v_y \tag{3}$$

$$D_{a,u} = v_u - v_y. \tag{4}$$

To complicate the definition of ductility, multiple methods to determine the yielding point exist. In [38], it was found that the value of the yielding point based on the modified method of EN 12512 [39] is the most appropriate since it gives the most suitable yielding point compared to the other methods. According to EN 12512 [39], the yielding point is found as the intersection between the initial stiffness K_{in} and the tangential stiffness to the graph with an inclination equal to $\frac{1}{6} \cdot K_{in}$. However, this gives a point that is not situated on the graph and, therefore, a modified version, where this point is projected onto the curve, was proposed. Regarding v_f, in [40], it is suggested to take the displacement at 98% of the maximum load or as the displacement at failure, while in EN 12512 [39], it is suggested to take v_f as the displacement at failure, as the displacement at 80% of the maximum force F_u, or as 30 mm, whichever occurs first. The present paper will refer to these two last definitions of v_y and ultimate displacement v_f to evaluate the ductility of timber joints.

In [40], an approach to classify fasteners in timber structures based on ductility ratios is provided (see Table 1). The limits are based on the indications contained in Eurocode 8 [11]. The classification creates the possibility of grouping certain joints based on their load-displacement behaviour:

Table 1. Classification of relative and absolute ductility.

Classification	**Relative *D*** **[-]**	**Absolute *D*** **[mm]**
Brittle	$D_{r,f} \leq 2$	$D_{a,f} \leq 1$
Low ductility	$2 < D_{r,f} \leq 4$	$1 < D_{a,f} \leq 3$
Moderate ductility	$4 < D_{r,f} \leq 6$	$3 < D_{a,f} \leq 6$
High ductility	$D_{r,f} > 6$	$D_{a,f} > 6$

The absolute values and the shape of the load-displacement curve of the joints can show considerable differences and depend not only on the type of fastener and joint configuration but also on several other parameters. These parameters can be grouped as follows:

- **geometrical parameters**: the fastener diameter, the type of fastener, the thickness of the timber members, the tolerances and the edge and end distances, the embedment or anchorage length and the spacing, the hole clearance, and the off-centring of the fasteners.
- **material parameters**: the density of the timber, the steel grade, the moisture content, the timber product wood species, the failure model, and the glue type.
- **loading and environmental parameters**: the load-to-grain angle, the load-to-surface angle, the load-to-fastener angle, monotonic or cyclic loading, the loading speed and load duration, the temperature, the moisture content, and the change in moisture content

The diverse shapes of the load-displacement curve are discussed in the following sub-sections, linking them, when possible, to the parameters of influence or the underlying physical phenomena.

2.2. Dowels and Bolts

In the case of joints with dowels and bolts, typical load-displacement curves may show all three previously identified regions (Figure 1). Some examples of typical shapes of the load-displacement curves of such joints are shown in Figure 2. These curves are representative of joints with dowels in double shear. In the case of bolted joints or steel-to-timber joints with dowels, the curve usually includes a more pronounced region of "zero stiffness" (curve D1 or D2 in Figure 2) compared to other types of fasteners, such as STS [32]. In fact, hole clearance and tolerances are responsible for the presence of a zero-stiffness region in the load-displacement curve [32] due to the delayed contact between the wood and the fasteners. This effect is diminished with the increasing number of fasteners in the joint due to the compensation of the stochastic arrangement [32], but is not fully eliminated. The joint may, under some circumstances, fail before entering the plastic region, showing only an elastic response up to failure (curve D1 in Figure 2). This happens when the joint is unable to exploit its full "potential" if its load-carrying capacity and ductility are limited by brittle timber failure (splitting, plug shear failure, block shear, etc). Brittle failure happens due to limited edge distances or, in the case of multi-fastener joints, to limited spacing. If the spacing or edge distances are reduced, the general shape of the curve stays the same and the failure point will be located at different positions along the curve. However, in this case the stiffness in the elastic branch remains unaffected [31,41,42]. For example, when the spacing is increased from 3d to 7d, the load-displacement curve can go from curve D1 to curve D2 in Figure 2. In general, in a multi-fastener joint, the load-carrying capacity and the ductility might also be limited by the failure mode of each fastener. In fact, the ductility decreases with decreasing values of the slenderness ratio, defined as the ratio between the embedment length and the diameter of the fastener. With increasing slenderness of the fasteners, whether it is due to a change in diameter or in the embedment length, the embedment capacity of the timber in the contact area to the fastener increases in relation to the yield capacity of the fastener. As a result, the displacement capacity and the plastic region of the load-displacement curve increase with increasing slenderness as long as timber failure is avoided [31].

In the plastic region, the curve can show a plastic plateau with clear identification of the maximum load-carrying capacity (curve D2 in Figure 2), it can show a hardening branch with an increase in load (curve D3 in Figure 2), or it can terminate with a softening branch (curve D4 in Figure 2).

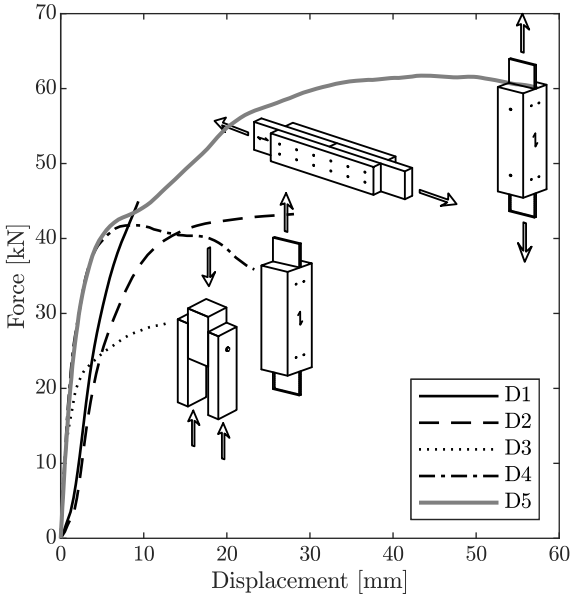

Figure 2. Curves of joints with dowels or bolts as fasteners. Details of the joint are reported in Table 2.

Table 2. Characteristics of joint represented in Figure 2.

Name	Type	Timber	Diameter [mm]
D1 [41]	Multi-dowel timber-timber	Solid timber	11.75
D2 [41]	Multi-dowel timber-timber	Solid timber	11.75
D3 [33]	Single-bolt timber-timber	Solid timber	12
D4 [43]	Single-dowel slotted-in plate	Glulam	16
D5 [43]	Single-dowel slotted-in plate and reinforcement	Glulam	16

Load-displacement curves with a hardening branch are typical for joints with fasteners whose ends are fixed, i.e., for bolts, due to the increased load from the rope effect with increased fastener displacement [44], which is similar to curve D3 in Figure 2. Similar shapes, i.e., characterized by hardening , can be found in joints loaded perpendicular to the grain. In fact, the load-displacement curve of the embedment of dowels loaded perpendicularly to the grain shows a lower stiffness, but the hardening occurs at higher displacements compared to dowels loaded parallel to the grain where higher initial stiffness and a more flat plastic plateau is reached. This is also reflected in the load-displacement curve of the entire joint. The hardening behaviour is possibly due to the densification of the wood in the contact area below the dowel and a rope effect in the wood fibers that are loaded in tension parallel to the grain [45].

The reinforcement of joints against tension perpendicular to the grain prevents splitting, which enables the joint to reach larger displacements along the plastic region of the load-displacement curve [46], and, thus, leads to more ductile behavior of the joint [31]. In the case of an interaction between the reinforcement and the fasteners, the embedment of the fastener can be enhanced, which leads to an increase in the load-carrying capacity and possible hardening of the curve [43]. Adding reinforcement in a joint can transform the load-displacement curve, like D3 in Figure 2 in the load-displacement curve, similar to D5 in Figure 2. In the latter case, the load-displacement curve looks like D5 in Figure 2 that shows extended plastic displacement with hardening, making it difficult to clearly identify the maximum load-carrying capacity.

2.3. Glued-in Rods

Joints with axially loaded GiRs can show very high performance with respect to the load-carrying capacity and stiffness per unit of the connected cross-sectional area and can

outperform similar joints with laterally loaded dowel-type fasteners. However, GiR joints can exhibit a variety of complex and brittle failure modes, which is why they are in reality often much less ductile than joints with laterally loaded dowel-type fasteners. The possible failure modes of axially loaded GiR are defined in the 2022 draft of EC5 [47] as one of the following four modes: (1) failure of the adhesive in the bondline and its bond with the rod and timber, (2) shear failure of the timber adjacent to the bondline, (3) splitting of the timber departing from the GiR, or (4) timber failure of the member in the surrounding of the GiR, and (5) yielding of the rod. Only with the last listed failure mode can ductile behaviour be achieved.

The behaviour of laterally loaded GiRs is considered to be quite similar to dowelled or bolted joints [48], with the failure modes according to the EYM. The adhesive bond of the rod in the timber is typically neglected in this case.

The resulting load-displacement curves describing the behaviour of joints with GiRs can be quite different depending on the failure mode, as shown in the examples in Figure 3. The examples provided in Figure 3 are related to joints realized with solid timber and glulam and they do not apply to GiRs in CLT. The load-displacement curve of axially loaded GiRs can be characterized by an initial linear elastic component with very high stiffness, which originates from the stiff bond created by the adhesive. Depending on the design of the GiR and the resulting failure mode, the curve can be limited by a brittle failure with no plastic displacement (curve G1 in Figure 3, typical for a bondline or timber failure of rods inserted parallel to the grain) or by a peak followed by a softening branch (curve G2, typical for a bondline and timber failure of rods inserted perpendicular to the grain). Where the GiRs are designed for the ductile tensile capacity of the steel rods, the linear elastic part of the curve is followed by a ductile branch (curve G3 in Figure 3). The choice of the geometric and material properties of the rod, adhesive, and timber determines the failure mode, and, consequently, the ductility of joints with GiRs. For example, reducing the diameter of the rod (i.e., increasing its slenderness) and, hence, reducing the yield capacity of the rod, can lead to a more ductile failure mode [49]. In contrast, increasing the rod diameter with a constant anchorage length results in a higher relative increase in the rod capacity and can stimulate brittle failure modes [50,51]. Rods made of low- and medium-steel-grade rods typically have a higher displacement capacity and a greater ratio between the ultimate strength and the yield strength compared to rods made of a high steel grade and, hence, are recommended for achieving ductility [52,53].

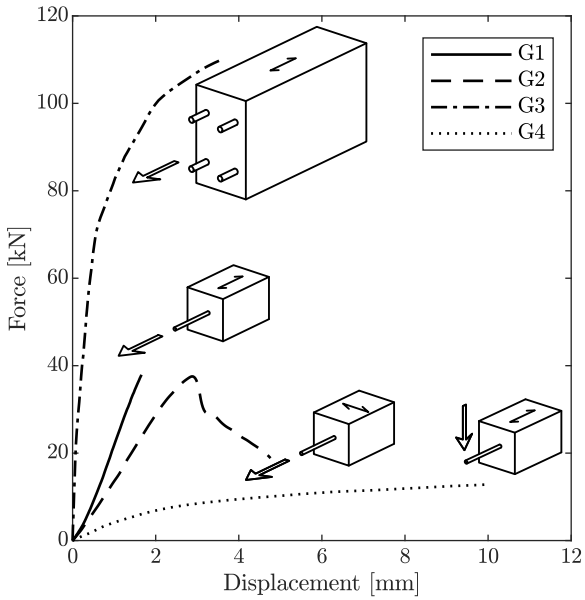

Figure 3. Examples of shapes of load-displacement curves of joints with GiRs. Characteristics of joints are reported in Table 3.

This ductility can be utilized to balance and equalize the possible non-uniform force distribution in joints with multiple GiRs and to utilize the full capacity of each GiR [54–56]. In order to achieve a desired displacement, a sufficient free unbounded length of the steel rod should be provided [57,58].

Laterally loaded GiRs do not benefit from high stiffness of the adhesion in the bondline and can show very soft and ductile behaviour (curve G4).

Table 3. Characteristics of GiR joint represented in Figure 3.

Name	GiR	Loading and Application Angle	Timber	Diameter [mm]	Length [mm]
G1 [59]	1	Axial, parallel to grain	LVL	12	150
G2 [59]	1	Axial, perpendicular to grain	ST	12	150
G3 [52]	4	Axial, parallel to grain	ST	20	300
G4 [60]	1	Lateral, parallel to grain	ST	16	320

2.4. Self-Tapping Screws (STS)

Depending on the application and configuration, joints with STS show different behaviours and have diverse shapes of load-displacement curves (Figure 4). For timber-to-timber joints, the zero stiffness region is much less pronounced since the STS are typically inserted without predrilling. The same applies to steel-to-timber joints with STS as long as the screw head fits tightly into the steel plate [32]. The load-displacement curve is nonlinear from the beginning, characterized by plastic hardening induced by the rope effect (curve S1 in Figure 4). It can also show stiff behaviour followed by an almost linear softening branch in the plastic region (curves S2 and S3 in Figure 4).

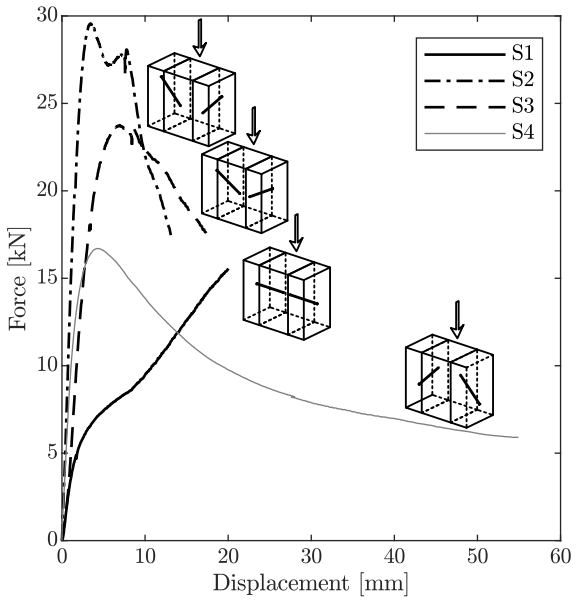

Figure 4. Examples of shapes of load-displacement curves of joints with STS in shear with different load-to-screw axis angles. Characteristics of the joints are reported in Table 4.

Table 4. Characteristics of STS joint represented in Figure 4.

Name	Type	Timber	Diameter [mm]	Load-to-Screw Axis Angle
S1 [61]	Timber-to-timber joints	Glulam	13	90
S2 [61]	Timber-to-timber joints	Glulam	13	45
S3 [61]	Timber-to-timber joints	Glulam	13	60
S4 [62]	Timber-to-timber joints	Glulam	8.2	−45

S4 in Figure 4 is a similar curve to S2 and S3, but in this case the displacements have been recorded to a large extent. In this case the softening branch is more complex and nonlinear.

Experiments on STS are not very numerous in the literature. However, joints with laterally loaded STS behave as laterally loaded dowels. Therefore, it can be assumed that joints with dowels and bolts and joints with laterally loaded STS share the same influential parameters. The particular characteristics of the screws become dominant as soon as the screws are loaded by a component in the axial direction.

2.5. Summary of Connection Behaviour

As discussed in the previous sections, the load-displacement behaviour of timber joints with dowels, bolts, GiRs, and STS is very diverse and can be highly nonlinear, which should be reflected in the assumptions made in design. However, in the current design codes, such as EC5, a rather simplistic, uniform and mostly linear elastic load-displacement behaviour is considered for joints. The existing nonlinearity means that a considerable difference between the initial elastic stiffness K_{ser} and the stiffness K_u at ULS at maximum load and/or maximum displacement exists.

The evolution of secant stiffness K_{sec} in relation to the secant stiffness (K_{1040}) to $0.10 \cdot F_u$ and $0.40 \cdot F_u$ (as suggested in [63]) is shown in Figure 5 for the load-displacement curves from Figures 2–4 in relation of the load level in the joints. The load level is defined as the ratio of the load value at which the secant stiffness is calculated, divided by the ultimate load F_u. The latter is defined as the maximum force or the force at a displacement of 15 mm, whichever occurred first. In the elastic range of the represented joints, the ratio $\frac{K_{sec}}{K_{1040}}$ is approximately 1 for all the joints. The value of the ratio $\frac{K_{sec}}{K_{1040}} = \frac{2}{3}$ that is assumed by EC5 for the ratio at the ultimate limit state is, in most cases, reached in the range of 60–100% of F_u, except for load-displacement curves characterized by a brittle failure mode, when the ratio stays around 1 up to F_u (see curves G1 and G2). Assuming that the joint will attract less load than in reality at the ultimate limit state can be an unsafe assumption in the case of a statically indeterminate structure, leading to an increased probability of failure [12].

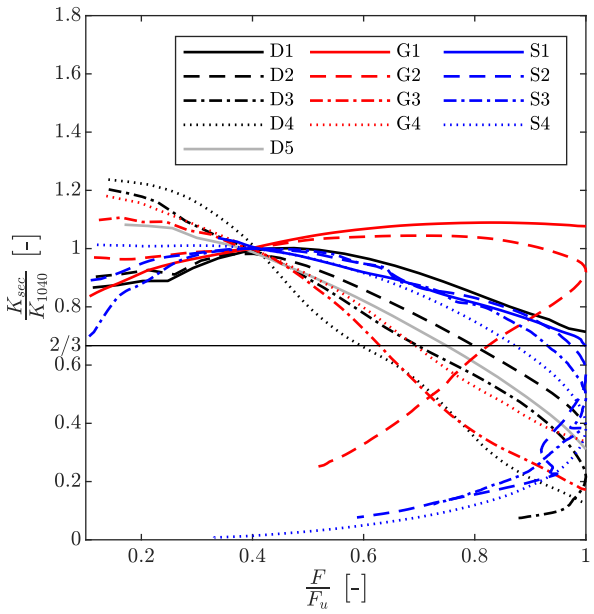

Figure 5. Relation of secant stiffness K_{sec} to secant stiffness $K_{sec,1040}$ along different load levels of the representative load-displacement curves.

The relative $D_{r,f}$ and absolute $D_{a,f}$ ratios of all the previously shown load-displacement curves are reported in Figure 6. The yielding point is identified based on a modified version of EN 12512 [39] and the used definition of ductility corresponds to Equations (1) and (3).

v_f was taken as the point that corresponds to the the failure, a load drop of $0.2 \cdot F_u$, or a maximum displacement of 30 mm, whichever occurred first (as indicated in [39]).

In general, fasteners in timber structures show low to high ductile behavior (see Figure 6). Even joints with GiRs, where the bondline behaviour is stiff and brittle, can show some ductility, if properly designed for yielding of the steel rods. However, it can be seen that it is necessary to differentiate between the relative value D_r and the absolute value D_a for some curves, for example, D2 of Figure 2. In that case, according to the absolute ductility definition, it is classified as a high ductile joint, while for relative ductility, it is classified as a low ductility joint. Figures 5 and 6 show that the mechanical behaviour of the joints is highly nonlinear. This shows that the formulas for the load-carrying capacity and the stiffness of joints given in EC5 are not sufficient to represent the behaviour of modern timber joints in the structural analysis of timber structures.

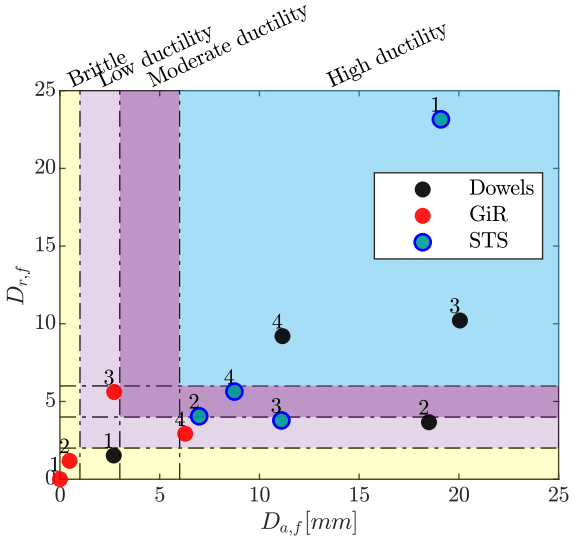

Figure 6. Interaction of the relative $D_{r,f}$ and absolute $D_{a,f}$ consideration of the ductility ratio. The value for curve D5 is excluded from the representation since it exceeds the representation intervals ($D_{r,f}$,$D_{a,f} \geq 25$). A similar graph can be found in [38].

Therefore, more precise and realistic descriptions of the load-displacement curves of timber joints, including the ductility also, are needed. In the following section, different analytical models are presented, and their suitability to model the diverse and complex joint behavior is evaluated.

The curves selected for further analysis are the ones that show more ductile behavior and more diverse shapes: curve D5 as a curve with a plastic plateau and a complex shape, D3 as a curve with a hardening branch, S1 as a curve with a strong hardening effect after the yield point, and S3 as a curve with a highly nonlinear softening branch. The curves D2 and D4 were selected to study the sensitivity of the regression models to the approximation of the initial slip and the displacement range, respectively. The curves that show brittle and, in general, less nonlinear behavior have been excluded since the analyzed models are expected to represent the brittle curves easily and in a comparable way. The selected load-displacement curves are represented in Figure 7:

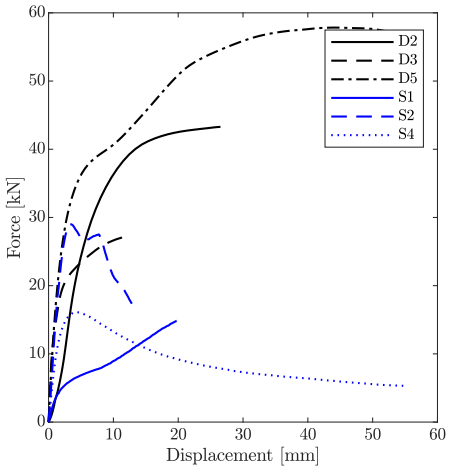

Figure 7. Load displacement shapes considered for the analysis.

3. Analytical Models and Regression Analysis

Analytical models to approximate the load-displacement behavior of joints, not limited to timber, have been proposed previously [13–17]. In this work, five types of models are selected for evaluation: the Foschi and Richard–Abbott models (based on exponential and power functions), and the Glos and Brander models (based on rational functions), and polynomials of different degrees. The model proposed in [16] was not analyzed since the parameters defining the model can only be obtained through solving complex nonlinear systems of equations and not through nonlinear regression.

3.1. Regression and Determination of Model Parameters

In this paper, the analytical models are fitted to the test data by performing regression along a certain region of the curve.

The problem is cast as:

$$\min_{a_1,a_2,\ldots,a_n} \sum_i (F(v_i; a_1, a_2, \ldots, a_n) - y_i)^2, \tag{5}$$

where $F(v_i; a_1, a_2, \ldots, a_n)$ is the value of the specified regression model that is dependent on the displacement values v_i and on a set of n parameters $a_1, a_2, \ldots, a_n$ (with n depending on the model), and y_i is the i-th component of the load vector.

3.2. Foschi and Richard–Abbott Models

Two commonly used analytical models to approximate the behavior of joints are the Foschi and the Richard–Abbott models [13,15]. Both models provide a physical interpretation of the parameters. The analytical model of Foschi [13] was initially developed for approximation of the load-displacement behavior of laterally loaded nails. It was later used for many different types of joints, even in steel structures. The model is defined as follows:

$$F(v) = (F_t + K_p \cdot v)(1 - e^{(\frac{-K_{in} \cdot v}{F_t})}) \tag{6}$$

where K_{in} is the elastic stiffness and K_p is the post-elastic stiffness. The y-intercept of the regression line of K_p is defined as F_t.

The Richard–Abbott model was developed to approximate nonlinear load-displacement or moment-rotation behavior in the analysis of nonlinear structural systems [15]. It was applied in steel structures and even in timber structures to approximate the embedment behavior at different load-to-grain angles [18]. It shares with the the Foschi model three parameters: K_{in}, K_b and F_t. The parameter a_1 is introduced to "regulate" the shape of the curve and to give the model more flexibility. The model can be described as follows:

$$F(v) = \frac{(K_{in} - K_p) \cdot v}{(1 + (\frac{(K_{in} - K_p)}{F_t})^{a_1})^{\frac{1}{a_1}})} + K_p \cdot v. \quad (7)$$

An illustration of the model shape, together with a representation of the parameters for both models, and the impact of the shape parameter a_1 of the Richard–Abbott model, are given in Figure 8.

In the model of Foschi, the first derivative is monotonically decreasing, approaching, for increasing displacement values, a value equal to K_p. Depending on whether the post-elastic branch of the load-displacement curve is characterized by softening, hardening, or perfect plasticity, the stiffness K_p is either negative, positive, or zero, respectively. At the beginning, the first derivative of the Richard–Abbott model decreases faster than that of the Foschi model. This trend changes after the point of intersection: the derivative of the Richard–Abbott model approaches the value K_p faster than the Foschi one (Figure 9).

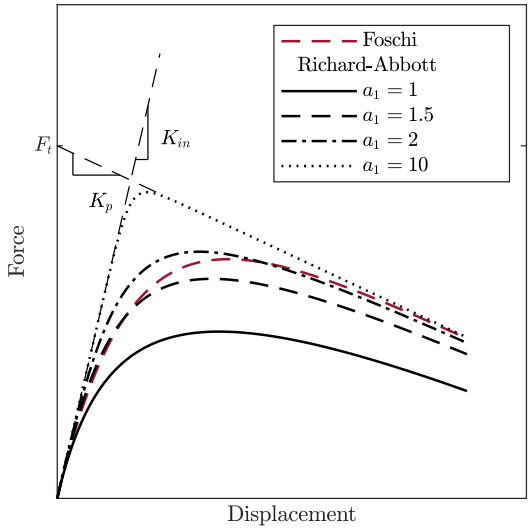

Figure 8. The Foschi and Richard–Abbott models [13,15].

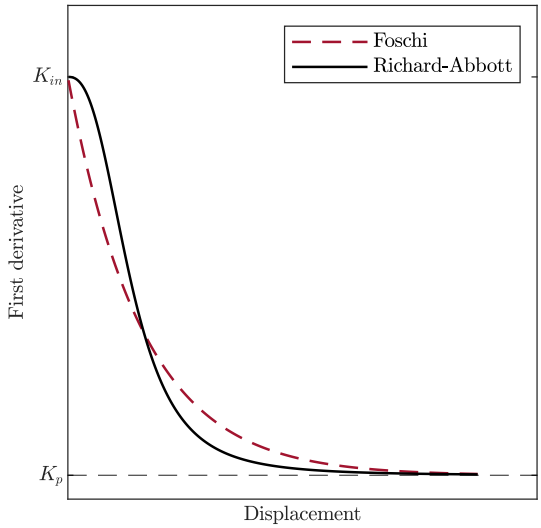

Figure 9. First derivative of the Foschi and of the Richard–Abbott models $a_1 = 3$.

3.3. Polynomial Model

Models based on polynomial functions can be fitted to different curves and provide, in general, one direct and unique solution. The Weierstrass approximation theorem states

that every continuous function (on a closed interval) can be approximated by a polynomial function [64]. Consequently, it can be assumed that every arbitrary (continuous) experimental curve can be described (or at least be well-approximated) by a polynomial function with the following equation:

$$F(v) = \sum_{n=1}^{k} p_i v^i. \tag{8}$$

The coefficients of Equation (8), in contrast to the Foschi and Richard–Abbott models, possess no physical interpretation.

3.4. The Models of Glos and Brandner

Glos and Brander [14,17] proposed two different models based on rational functions, whose coefficients are determined by imposing boundary conditions. The rational functions are flexible, but they might be discontinuous in correspondence to the roots of the denominator.

The model of Glos was developed to simulate the behavior of timber in compression parallel to the grain. The corresponding mathematical function is given in Equation (9):

$$F(v) = \frac{v + c_1 \cdot v^{c5}}{c_2 + c_3 \cdot v + c_4 \cdot v^{c5}}. \tag{9}$$

The values of the coefficients c_1 to c_4 can be determined from the characteristics of the load-displacement curve through the application of the boundary conditions in Equations (10)–(13) while the coefficient c_5 is a shape parameter. K_{in} corresponds to the initial stiffness of the curve, v_u is the displacement at the maximum load F_u, and K_u is the (tangential) stiffness of the curve at that point. The value of K_u is typically close to 0. F_a is the load level asymptotically approximated at large displacements v. The function and the derivative are illustrated in Figures 10 and 11, respectively.

$$\frac{\mathrm{d}F}{\mathrm{d}x}(v = 0) = K_{in} \tag{10}$$

$$\frac{\mathrm{d}F}{\mathrm{d}x}(v = v_u) = K_u \tag{11}$$

$$F(v = v_u) = F_u \tag{12}$$

$$F(v \gg v_u) = F_a \tag{13}$$

The resulting equations for the determination of the coefficients are given in Equations (14)–(17).

$$c_1 = \frac{F_a}{(c_5 - 1) \cdot K_{in} \cdot v_u^{c_5} \cdot (1 - \frac{F_a}{F_u})} \tag{14}$$

$$c_2 = \frac{1}{K_{in}} \tag{15}$$

$$c_3 = \frac{1}{F_u} - \frac{c_5}{K_{in} \cdot v_u \cdot (c_5 - 1)} \tag{16}$$

$$c_4 = \frac{1}{(c_5 - 1) \cdot K_{in} \cdot v_u^{c_5} \cdot (1 - \frac{F_a}{F_u})} \tag{17}$$

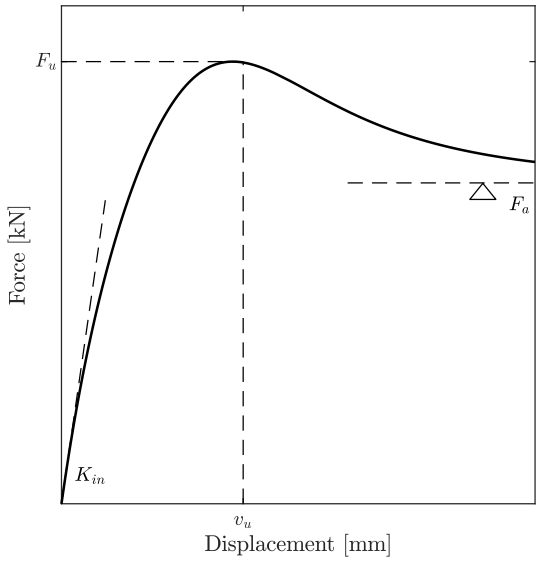

Figure 10. The Glos model.

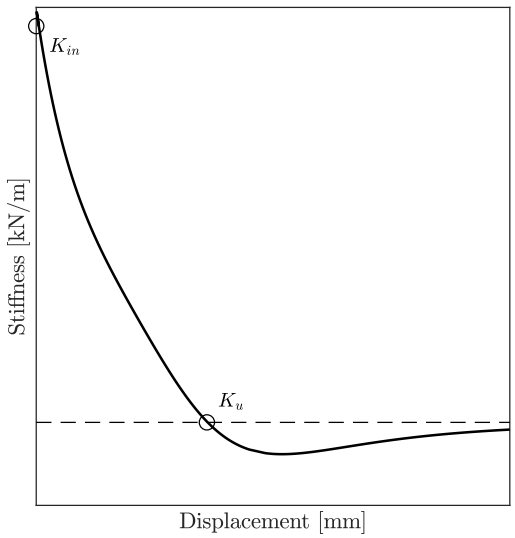

Figure 11. The first derivative of the Glos model.

The Brandner model is a modification of the model proposed in Glos [14] by the addition of an initial linear branch between v_{in} and v_{lin}, as shown in Figure 12 (cf. Equations (18) and (19)), in order to describe the withdrawal load-displacement curve of single self-tapping screws in CLT. Furthermore, the Brandner model offers the possibility to consider the initial slip (v_{in}) by shifting the simulated load-displacement curve horizontally to the extent of v_{in}.

$$F(v = 0) = v \leq v_{ini} \tag{18}$$

$$F(v = 0) = K_{in} \cdot (v - v_{in}) \tag{19}$$

The resulting equation of the Brandner model is:

$$F = \frac{v}{c_1 + c_2 \cdot (v - v_{in}) + c_3 \cdot (v - v_{in})^{c_4}}. \tag{20}$$

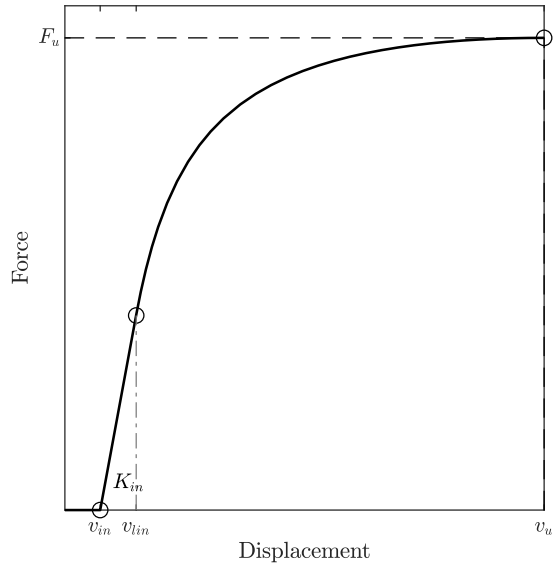

Figure 12. The Brandner model [17].

To ensure a smooth transition between the initial linear elastic and the nonlinear part of the curve, the slope of the curves needs to be the same as illustrated in Figure 13. Since the residual resistance at large displacement is not considered in the model, the asymptotic load level of the softening branch is set to zero ($F_a = 0$). Thus, one coefficient of the Glos model disappears; the modified equations for calculating the coefficients c_1 to c_3 of Equation (20) are defined as follows:

$$c_1 = \frac{1}{K_{in}} \tag{21}$$

$$c_2 = \frac{1}{F_u - K_{in} \cdot (v_{lin} - v_{in})} - \frac{c_4}{K_{in} \cdot (v_u - v_{lin}) \cdot (c_4 - 1)} \tag{22}$$

$$c_3 = \frac{1}{(c_4 - 1) \cdot K_{in} \cdot (v_u - v_{lin})^{c_4}}. \tag{23}$$

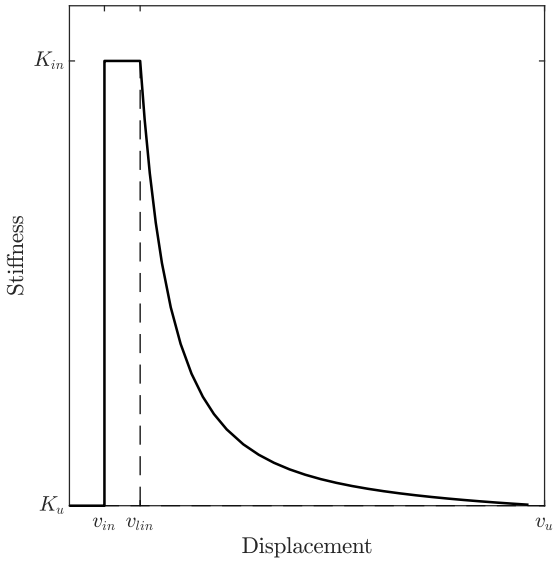

Figure 13. The first derivative of the Brandner model [17].

4. Results and Discussion

4.1. Model Application and Evaluation

In this section, the models of Foschi, Richard–Abbott, Glos, and Brandner, as well as the polynomial, are applied to the curves in Figure 7 and the performances of these models are compared and evaluated in Section 4.2.

The initial slip of the curves, when present, is removed by shifting the curve to the intercept at v_{in}, as illustrated in Figure 14. When the initial slip is removed, the initial part of the curve up to a force $F = 0.1 \cdot F_u$ is removed and replaced by a linear section with an inclination equal to the secant stiffness through the curve at $0.10 \cdot F_u$ and $0.40 \cdot F_u$ (see Figure 14). A more detailed study on the ability of the models to capture the initial slip region is performed for the curve D2 for dowel joints in Section 4.2.2.

The regression analysis was performed by application of least square fitting up to the smaller of either the maximum recorded displacement or the displacement corresponding to a load drop to or below $0.6 \cdot F_u$. A more detailed study on the impact of the displacement range on the performance of the models was performed for curve S4 in Section 4.2.3.

The sensitivity of the models to variability in the experimental data is evaluated in Section 4.3.

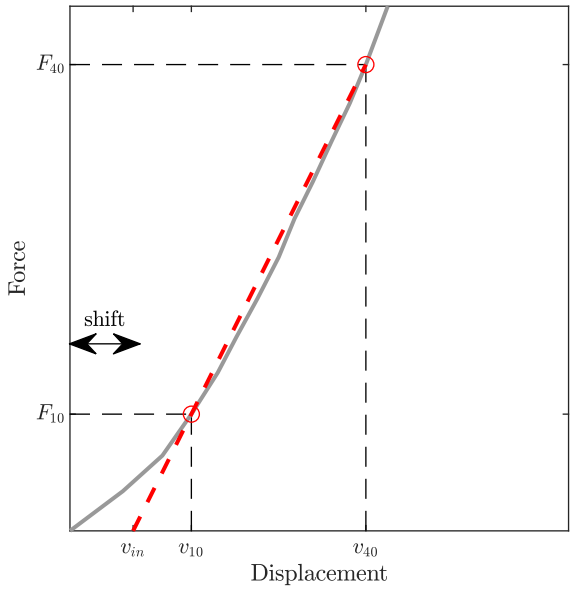

Figure 14. Initial shift of the curves.

4.2. Regression and Model Fit to the Load-Displacement Curves of Timber Joints

4.2.1. General Model Fit

Three distinctly different nonlinear load-displacement curves were selected to evaluate and to highlight the main differences between the performance of the regression models. The three curves and the model comparison are shown in Figure 15. The experimental curves show different behavior in the plastic region: the curve represented in Figure 15a is characterized by the simultaneous presence of two plastic plateau, the curve in Figure 15b is characterized by a strong hardening effect, and the curve in Figure 15c shows a complex softening branch.

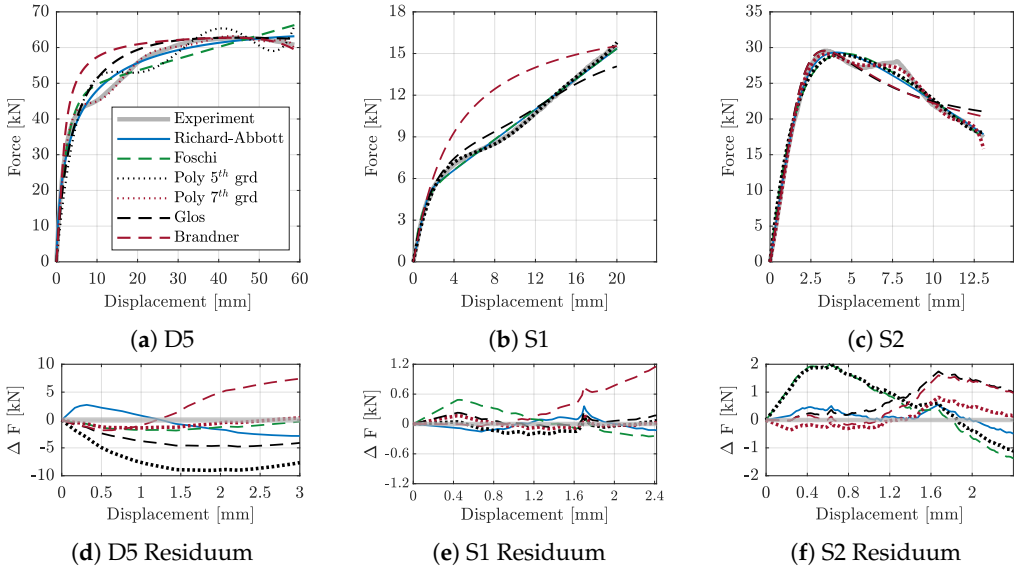

Figure 15. Application of parametrization equations to different types of experimentally determined slip curves.

For the evaluation of the models' performances for regression of the experimental data, the absolute error of the regression with respect to the experimental data was determined and is illustrated in Figure 15d–f. In particular, the residuum is illustrated only in the elastic displacement range up to the displacement corresponding to the yielding point to show in detail how the regression model approximates the first part of the curves. The goodness of fit can be measured with a standard coefficient of determination or an adjusted coefficient of determination. The adjusted coefficient of determination takes into account the number of parameters of the model and the quantity of experimental data. The two coefficients were compared, but no remarkable differences were found between the them; thus, the goodness of fit was measured by the standard coefficient of determination R^2 for all the analyzed curves and is illustrated in Figure 16.

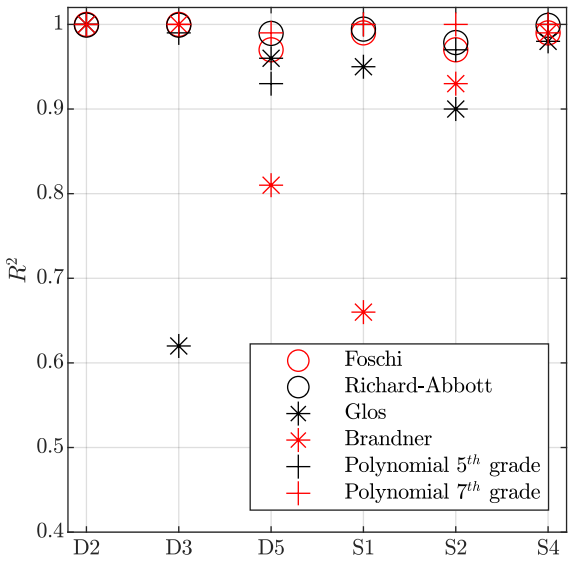

Figure 16. R^2 coefficient for all the curves and regression models.

The Foschi model has the advantage of reflecting a physical meaning of the coefficients, allowing easy interpretation of the coefficients in relation to the other parameters. Looking at the derivative graph of the Foschi model, it can be observed that the curve decreases (asymptotically) with a nonlinear trend, from an initial stiffness value to a plateau. The stiffness value of this lower stiffness plateau can coincide with the hardening stiffness for curve S1 or the softening stiffness for curve S2. The shape of the transition cannot be influenced in the Foschi model. Therefore, the model looks more suitable for the curve of S1, where an elastic branch with a constant inclination can be hardly determined since the load-displacement curve is highly nonlinear from the beginning (see Figure 15a,d). The least squares, when used to determine the three parameters, tend to overestimate the initial stiffness. Although the model was originally developed for a curve similar to S1, it is nonetheless able to provide a satisfactory approximation of the load-displacement curve with a softening branch. However, the softening behavior can only be approximated linearly.

The Richard–Abbott model has an additional parameter compared to the Foschi model. This makes the model more flexible. It overestimates slightly the initial part of the curve for all the selected curves, however, less so than the Foschi model. When applied to D5 (see Figure 15a), however, the Richard–Abbott model overestimates the initial stiffness compared to Foschi (see Figure 15d). In the plastic region of the curve D5, the Richard–Abbott and Foschi models show continuous hardening behavior that does not appear in the experimental curve. This is due to the complex shape of the curve that the Foschi and Richard–Abbott models are too rigid to approximate precisely. Like the Foschi model, the Richard–Abbott model can only approximate the softening branch linearly.

A polynomial function of the 5th degree was fitted to the experimental curves in Figure 15. This polynomial model provides a good approximation of all the analyzed curves, except for the curves D5 and S2. In fact, the polynomial model turns out to be wavy, and does not provide a satisfactory approximation of the curve in the plastic region. In order to overcome this issue, the degree of the polynomial was increased until a perfect approximation of the curve was obtained for curves D5 and S2 and the waves were eliminated. This was achieved for a polynomial of the 7th degree for both curves. This illustrates the flexibility of the polynomial model to also represent the complex shapes of curves. However, the good fit and model performance should not be achieved only by increasing the number of coefficients in the model. The coefficients of the Glos and the Brandner models are determined by imposing specified boundary conditions. However, for the case of the curve S1, the local maximum of the curve is absent. In order to be able to apply the models, the local maximum has been replaced by the yielding point. For the determination of this point, the modified definition provided in [39] was used.

Nevertheless, the models of Glos and Brandner show a poor fit and are not suitable to represent curves with hardening, such as S1.

4.2.2. Influence of the Initial Region

Models like the Foschi and Richard–Abbott models do not explicitly take into account the presence of initial slip in the curve. The only model that explicitly takes this region into account is the Brandner model. The Brandner model approximates the region of initial slip by considering a shift of the curve equal to v_{in}, corresponding to a zero force. Such a shift can be considered for the other models too, such as the Richard–Abbott or Foschi models. The polynomial model, since its coefficients are non-physical, is able to approximate the initial region of zero stiffness through an increase in its grade. The Glos model does not take into account any initial slip; however, as a rational function, it is very flexible, and, when applied on curves without softening, it can be adapted to also include the initial slip.

In order to evaluate the impact of the initial slip region on the model fit, the models by Brandner, Glos, and Richard–Abbott, as well as the polynomial of the 5th and 6th were tested on curve D2 without removing the initial slip. The results are illustrated in Figure 17. The Brandner model is the easiest way to include an initial slip through an approximation. The model by Glos enables precise following of the initial slip region of the curve, which, however, results in major differences in the further elastic region of the curve.

The manual shift of the Foschi and Richard–Abbott models is an alternative way to consider the initial slip and to achieve a good model fit (Figure 17).

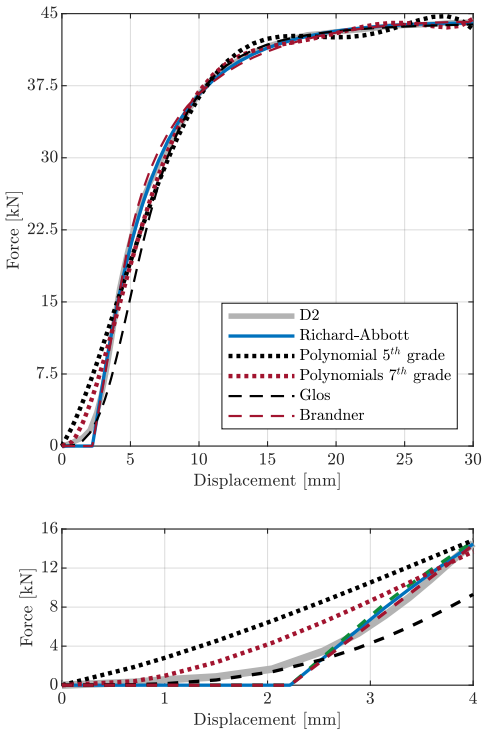

Figure 17. Regression applied to D2.

4.2.3. Influence of the Displacement Range

The quality of the regression performance of the models is sensitive to the displacement range considered, as illustrated in Figure 18. To test the sensitivity of the regression models to the displacement range, the models were applied to curve S4 with different displacement ranges. The sensitivity of the Foschi model to the displacement range was similar to that of the Richard–Abbott model and the sensitivity of the Brander model was similar to that of the Glos model. For this reason, only the models of Richard–Abbott, Bradner, and the polynomial of the 5th grade are illustrated. Increasing the grade of the polynomial makes the model less and less sensitive to the displacement range. The Richard–Abbott model is more sensitive to the displacement range than the Glos model. In particular, for the maximum recorded displacement case (60 mm), the model is not able to approximate the maximum point satisfactorily. The Glos model remains more or less stable, while the polynomial already becomes unstable at a displacement corresponding to $0.5 \cdot F_u$. For the polynomial, the quality of the fit worsens even in the elastic zone: the initial slope is underestimated with increasing displacement range.

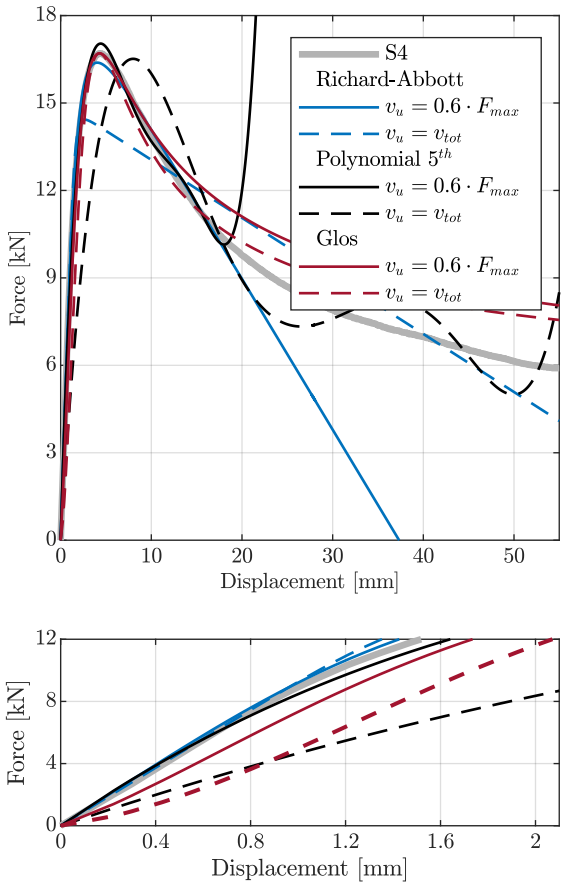

Figure 18. Impact of the displacement range on the quality of the regression.

4.3. Stability of the Regression Model

Based on the discussion in the previous section, two models showed good performance on all the analyzed curves: the Richard–Abbott and the polynomials. The Richard–Abbott model has the advantage of a limited number of parameters, while the model based on polynomials, if a high degree is selected, is able to approximate even very complex shapes. One of the goals of using parametrized models for the description of the load-displacement behavior of timber joints is to be able to better compare the behavior of different joint typologies and to assess the variability in the behavior that is associated with the different parameters. The variability in the load-displacement behavior of the timber joints originates, amongst others, from the natural variability of the materials used and from the material properties related to the relevant failure mode. Hence, the variability in the load-displacement curves can differ according to the different failure modes of the joint. In particular, the failure modes in timber are associated with a larger variability, while the failure modes associated with steel result typically in less variability [42,65]. Also, variations and tolerances in the geometry and configuration, occurring during the assembly process in the case of timber joints, impact the variability of the load-displacement behavior.

The Richard–Abbott model and a polynomial model of the 7th degree were tested on available experimental data from [61] in terms of their stability to the intrinsic variability of the data. The selected experimental data were timber-to-timber joints with inclined STS, i.e., the series S1–S3 with a different number of specimens per series. The model is considered to be stable if a relatively small change in the data results in a small change in the estimated values of the parameters of the model. In particular, if the coefficient of variance (COV) of the analyzed model parameters is much larger than that of the data, the model is considered to be unstable, i.e., it is considered not to be able to properly capture the variability in the data.

In [61], experiments are reported on timber-to-timber shear joints with fully threaded screws of diameter $d = 13$ mm inclined with a different angle to the shear plane and for two different ranges of timber density: high density with $\rho_m = 464$ kg/m^3 and low density with $\rho_m = 350$ kg/m^3. The Richard–Abbott and polynomial models were individually fitted to all the experimental curves. For each of the model parameters, the mean value and the standard deviation were calculated and plotted as error bars in Figure 19. The symbol ◯ represents the values for the specimen group of high density and the symbol △ is used to represent the low-density group. The different colors black and blue are used when graphs with two scales are used.

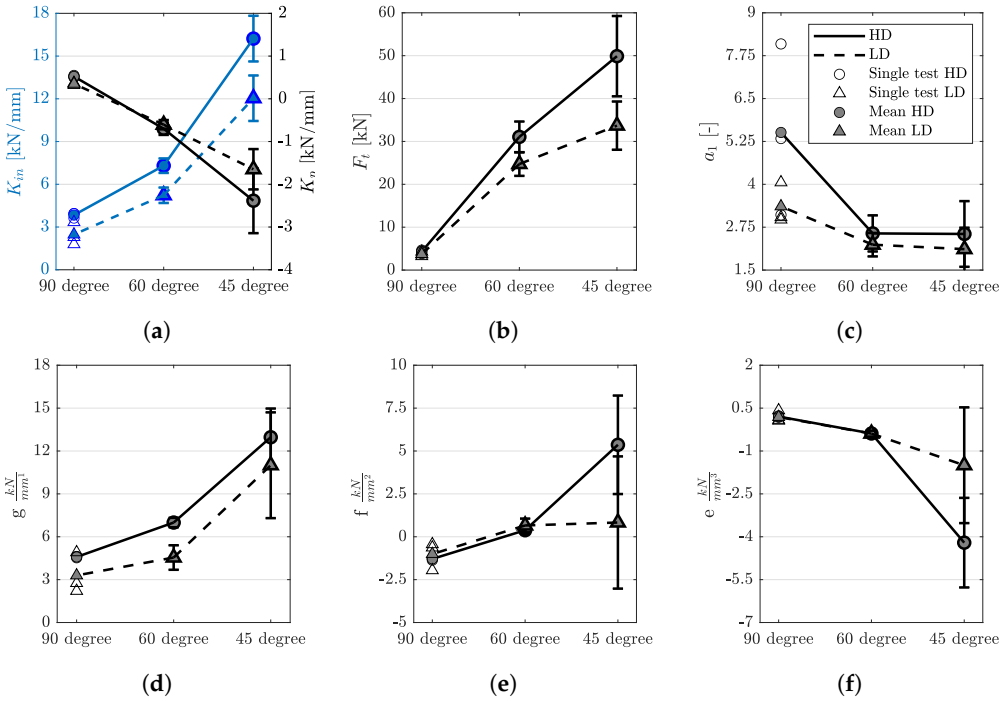

Figure 19. Variation in the model coefficients in dependency of the load-to-screw axis angle. (**a**) Richard–Abbott model: stiffnesses K_{in} and K_p; (**b**) Richard–Abbott model: force intercept F_t; (**c**) Richard–Abbott model: shape parameter a_1; (**d**) polynomial coefficient g of 7th grade; (**e**) polynomial coefficient f of 7th grade; (**f**) polynomial coefficient e of 7th grade.

The mean values and the respective CoVs are reported in Tables 5 and 6 for the groups of both high and low density. Due to the limited number of repetitions for the configuration with a load-to-screw axis angle of 90°, only the mean values are reported.

Table 5. Coefficients of the Richard–Abbott model for the data set on STS.

Angle [°]	n_{test}	K_{in} $\left[\frac{kN}{mm}\right]$ **(CoV)**	K_p $\left[\frac{kN}{mm}\right]$ **(CoV)**	F_t $[kN]$ **(CoV)**	α $[-]$ **(CoV)**
High density					
90	3	3.84	0.52	4.31	5.51
60	4	7.31 (7%)	−0.70 (21%)	31.06 (12%)	2.57 (20%)
45	7	16.22 (10%)	−2.38 (32%)	49.88 (19%)	2.55 (38%)
Low density					
90	3	2.48	0.35	3.73	3.36
60	4	5.23 (10%)	−0.61 (18%)	24.73 (11%)	2.24 (15%)
45	8	12.04 (13%)	−1.64 (29%)	33.69 (17%)	2.11 (30%)

Table 6. Coefficients of 7th grade polynomial model for the data set on STS.

Angle [°]	a $\frac{kN}{mm^7}$	b $\frac{kN}{mm^6}$	c $\frac{kN}{mm^5}$	d $\frac{kN}{mm^4}$	e $\frac{kN}{mm^3}$	f $\frac{kN}{mm^2}$	g $\frac{kN}{mm^1}$
			High density				
90	3.29×10^{-7}	-2.74×10^{-5}	9.73×10^{-4}	-2.04×10^{-2}	0.20	−1.29	4.57
60	-2.09×10^{-6} (44%)	1.52×10^{-4} (39%)	-4.36×10^{-3} (34%)	0.06 (29%)	−0.39 (26%)	0.38 (59%)	7 (5%)
45	-1.46×10^{-4} (60%)	6.61×10^{-3} (52%)	−0.12 (46%)	1.01 (40%)	−4.21 (37%)	5.36 (54%)	12.96 (15%)
			Low density				
90	6.77×10^{-7}	-4.73×10^{-5}	1.36×10^{-4}	−0.021	0.19	−1.01	3.30
60	-2.28×10^{-6} (35%)	1.61×10^{-4} (31%)	-4.46×10^{-3} (27%)	0.061 (25%)	−0.39 (26%)	0.66 (61%)	4.55 (19%)
45	-2.17×10^{-5} (703%)	1.57×10^{-3} (347%)	-3.57×10^{-2} (215%)	0.35 (154%)	−1.50 (135%)	0.83 (463%)	11.00 (34%)

It can be noted that for the Richard–Abbott model, the mean value of the initial stiffness parameter K_{in} increases with increasing inclination of the fasteners (decreasing load-to-screw axis angle), while the post-elastic stiffness K_p decreases (Figure 19a). The mean value of the force-intercept F_t, which is graphically connected to K_p, increases with increasing inclination (Figure 19b). In fact, a lower value of K_p (stronger softening behavior) results in a higher intercept on the vertical (force) axis. The mean value of the shape factor a_1 decreases for a change in the screw inclination from 90° to 60°; however, it stays approximately constant between 60° and 45° (Figure 19c). An evident increase in variability with increasing inclination of the fastener can be observed for the coefficients K_p and F_t, which can be related to the different failure modes involved. When the STS are inclined at 90°, the failure is characterized by bending and yielding of the screws, whose material properties are characterized by a rather low variability [9]. When the screw is inclined and, thus, also axially loaded, the failure involves the withdrawal mechanism with shearing failure in the timber, with a typically higher variability. For K_{in}, no clear trend can be observed in the dependency of the failure mode and more tests are needed.

It is also possible to identify a generally positive impact of density on the parameters: the larger the density, the larger the mean values of the parameters. Only for the parameter K_p at angles of 90° and 60° can this not be confirmed.

The difference between higher and lower density increases with decreasing angle for K_{in}, K_p and F_t. The variability in the parameters is consistent for the two groups of low and high density, being in a range between 7% to 38%, that is not uncommon for timber properties. More experimental data are needed to confirm and clarify the observed trends and to determine more reliable values, in particular for a load-to-screw axis angle of 90°.

The parameters of the polynomial model are summarized in Table 6 and Figure 19d–f. A drastic increase in the scatter for the values of the coefficients at 45° can be observed in Figure 19e,f. Only coefficient *g* shows a positive correlation with the density and inclination (Figure 19d).

The scatter of the values of the coefficients is mostly very high and exceeds in many cases the variation in the parameters related to a change in the density group or inclination. This means that the variability in the coefficients is not related to the variability in the input data but is rather associated with the fitted noise.

The inconsistent trends of the coefficients, together with the large scatter, make it impossible to determine reliable coefficients for a set of data and their distribution characteristics for the polynomial model.

5. Summary and Conclusions

In this paper the load-displacement behavior of different types of timber joints were analysed and different parametric regression models were summarized and evaluated. The performance of the models was tested on a range of typical load-displacement curves, in particular, in terms of their ability to represent those curves with complex and highly nonlinear shapes. The Richard–Abbott and the polynomial model of the 7th degree were

selected and evaluated regarding their ability to capture variability in the data for the entire test series.

The following conclusions can be drawn with regard to the performance of the regression models on the typical load-displacement curves of timber joints:

- The models of Foschi and Richard–Abbott are comparably simple and showed good performance on curves with or without softening, and curves with an almost linear softening branch. The latter are too rigid to be able to achieve good regression for highly nonlinear post-elastic shapes (see, e.g., curves D5 or S2). However, these types of shapes, although present among the load-displacement curves of timber joints, are not the most common ones;
- The Brandner and Glos models have a more refined shape. The softening branch can be approximated with a nonlinear trend, in contrast to the Foschi and Richard–Abbott models. However, both models are not suitable to represent the load-displacement curves without softening branches, i.e., when displacement criteria are used as failure criteria and limit the test data (see, e.g., curve S1).
- The polynomial models of sufficiently high degree are able to approximate even highly complex shapes, such as those with a second plastic plateau or a highly nonlinear softening branch (see, e.g., curves D5 and S2).
- The initial slip can be included in all the models by adding an initial shift to the model curves. Only the models of Glos and the polynomials of enough flexibility offer the possibility to integrate the slip without breaking the continuity of the function;
- All the models, except the Glos and Brander models, are sensitive to the displacement range. Considering a displacement range that corresponds to more than $0.6 \cdot F_u$, would mean worsening the overall fit of the regression models;
- The stability of the Richard–Abbott model and the polynomial model of the 7th degree was tested on a data set from experiments with STS. Only the Richard–Abbott model was capable of representing the variability in the test data in its regression parameters, while the regression of the polynomial to the variable data led to considerable noise in the parameters.

The advantages and limitations of each model are summarized in Table 7.

It can be concluded that the Richard–Abbott model is a suitable model to parametrize the load-displacement behavior of different timber joints and to capture and quantify the related variability in the test data. Such a parametrized model can be used to integrate the description of the nonlinear load-displacement behavior of joints in structural design software, to perform reliability analyses of more complex structural systems, and to consider more precisely aspects such as the stiffness and ductility of joints in design codes. In order to achieve this, further research is necessary to quantify the model parameters and their distribution parameters on larger data sets for a variety of modern timber joints.

Table 7. Advantages and limitations of each regression model.

Model	Advantages	Limitations
Foschi	Physical interpretation of the parameters Limited numbers of parameters Manually determined parameters	Limited flexibility Sensitivity to the displacement range Linearization of softening branch Overestimation of initial stiffness Initial slip considered by shift
Richard–Abbott	Physical interpretation of some parameters Limited numbers of parameters Manually determined parameters	Limited flexibility (less than Foschi) Sensitivity to the displacement range Linearization of softening branch Slight overestimation of initial stiffness Initial slip considered by shift

Table 7. *Cont.*

Model	Advantages	Limitations
Glos	Limited numbers of parameters Nonlinear approximation of softening Possibility to represent nonlinear initial shift	No hardening representation No physical interpretation of parameters Possible presence of discontinuities No consideration of linear elastic branch
Brandner	Limited numbers of parameters Nonlinear approximation of softening Linear elastic branch representation	No hardening representation No physical interpretation of parameters Possible presence of discontinuities Initial slip considered by shift
Polynomial	Flexibility Large number of parameters Nonlinear approximation of softening Nonlinear approximation of initial slip	Wavy shapes No physical interpretation of parameters Sensitivity to the displacement range

Author Contributions: Conceptualization, methodology, formal analysis, investigation, data curation, writing—original draft preparation and writing—review and editing, D.C.; conceptualization, methodology, writing—original draft preparation, writing—review and editing, supervision, project administration and funding acquisition, R.J. All authors have read and agreed to the published version of the manuscript.

Funding: The financial support of this project by Svensk Trä, the Swedish association of the timber industries, and TMF, the Swedish Federation of Wood and Furniture Industry, is gratefully acknowledged.

Data Availability Statement: The data presented in this study are available on request from the corresponding author.

Conflicts of Interest: The authors declare no conflict of interest. The funders had no role in the design of the study; in the collection, analyses, or interpretation of data; in the writing of the manuscript; or in the decision to publish the results.

References

1. *NZS AS 1720.1:2022*; Timber Structures Part 1: Design Methods. Standards Association of Australia: Sydney, Australia; Standards New Zealand: Wellington, New Zealand, 2022.
2. Ottenhaus, L.M.; Jockwer, R.; van Drimmelen, D.; Crews, K. Designing timber connections for ductility—A review and discussion. *Constr. Build. Mater.* **2021**, *304*, 124621. [CrossRef]
3. Larsen, H.J.; Jensen, J.L. Influence of semi-rigidity of joints on the behaviour of timber structures. *Prog. Struct. Eng. Mater.* **2000**, *2*, 267–277. [CrossRef]
4. Crocetti, R. Large-Span Timber Structures. In Proceedings of the World Congress on Civil, Structural, and Environmental Engineering, Prague, Czech Republic, 30–31 March 2016; pp. 1–23. [CrossRef]
5. Malo, K.A.; Abrahamsen, R.B.; Bjertnæs, M.A. Some structural design issues of the 14-storey timber framed building "Treet" in Norway. *Eur. J. Wood Wood Prod.* **2016**, *74*, 407–424. [CrossRef]
6. Frühwald, E.; Serrano, E.; Toratti, T.; Emilsson, A.; Thelandersson, S. *Design of Safe Timber Structures—How Can we Learn from Structural Failures in Concrete, Steel and Timber?* Technical Report TVBK-3053; Division of Structural Engineering, Lund University: Lund, Sweden, 2007.
7. Hendawi, S.; Frangopol, D.M. System reliability and redundancy in structural design and evaluation. *Struct. Saf.* **1994**, *16*, 47–71. [CrossRef]
8. *EN 1995-1-1:2004*; Eurocode 5: Design of Timber Structures—Part 1-1: General—Common Rules and Rules for Buildings. European Committee for Standardization CEN: Brussels, Belgium, 2004.
9. Jockwer, R.; Caprio, D.; Jorissen, A. Evaluation of parameters influencing the load-deformation behaviour of connections with laterally loaded dowel-type fasteners. *Wood Mater. Sci. Eng.* **2021**, *17*, 6–19. [CrossRef]
10. Mack, J.J. *The Strength and Stiffness of Nailed Joints under Short-Duration Loading*; Division of Forest Products Technological Paper; Commonwealth Scientific and Industrial Research Organization: Melbourne, Australia, 1966.
11. *EN 1998-1:2004*; Eurocode 8: Design of Structures for Earthquake Resistance—Part 1: General Rules, Seismic Actions and Rules for Buildings. European Committee for Standardization CEN: Brussels, Belgium, 2004.
12. Caprio, D.; Jockwer, R.; al Emrani, M. Reliability of statically indeterminate timber structures: Modelling approaches and sensitivity study. In *Current Perspectives and New Directions in Mechanics, Modelling and Design of Structural Systems*; CRC Press: Boca Raton, FL, USA, 2022; pp. 1649–1655. [CrossRef]

13. Foschi, R.O. Load-slip characteristics of nails. *Wood Sci.* **1974**, *7*, 69–76.
14. Glos, P. Zur Bestimmung des Festigkeitsverhaltens von Brettschichtholz bei Druckbeanspruchung aus Werkstoff- und Einwirkungskenngrößen. Berichte zur Zuverlässigkeitstheorie der Bauwerke, No. 35/78. Ph.D. Thesis, Technische Universität München, Munich, Germany, 1978.
15. Richard, R.M.; Abbott, B.J. Versatile Elastic-Plastic Stress-Strain Formula. *J. Eng. Mech. Div.* **1975**, *101*, 511–515. [CrossRef]
16. Flatscher, G. *Evaluation and Approximation of Timber Connection Properties for Displacement-Based Analysis of CLT Wall Systems*; Monographic Series TU Graz: Timber Engineering & Technology; Verlag der Technischen Universität Graz: Graz, Austria, 2017; Volume TET 6.
17. Brandner, R.; Ringhofer, A.; Grabner, M. Probabilistic models for the withdrawal behavior of single self-tapping screws in the narrow face of cross laminated timber (CLT). *Eur. J. Wood Wood Prod.* **2018**, *76*, 13–30. [CrossRef]
18. Schweigler, M.; Bader, T.K.; Hochreiner, G.; Lemaître, R. Parameterization equations for the nonlinear connection slip applied to the anisotropic embedment behavior of wood. *Compos. Part B Eng.* **2018**, *142*, 142–158. [CrossRef]
19. Schweigler, M.; Bader, T.; Hochreiner, G. Engineering modeling of semi-rigid joints with dowel-type fasteners for nonlinear analysis of timber structures. *Eng. Struct.* **2018**, *171*, 123–139. [CrossRef]
20. Schilling, S. Structural Behaviour and Reliability of Timber Trusses with Dowelled Steel-to-Timber Connections. Ph.D. Thesis, ETH Zurich, Zurich, Switzerland, 2022. [CrossRef]
21. Abrahamsen, R.B. Bridge across Rena River—"World's strongest timber bridge". In Proceedings of the World Conference on Timber Engineering, WCTE 2008, Miyazaki, Japan, 2–5 June 2008; pp. 1–8.
22. Rebouças, A.S.; Mehdipour, Z.; Branco, J.M.; Lourenço, P.B. Ductile Moment-Resisting Timber Connections: A Review. *Buildings* **2022**, *12*, 240. [CrossRef]
23. Serrano, E.; Steiger, R.; Lavisci, P. Glued-in rods. In *Core Document of the COST Action E34 Bonding of Timber*; Technical Report; Universität für Bodenkultur Wien: Vienna, Austria, 2008.
24. Steiger, R.; Serrano, E.; Stepinac, M.; Rajčić, V.; O'Neill, C.; McPolin, D.; Widmann, R. Strengthening of timber structures with glued-in rods. *Constr. Build. Mater.* **2015**, *97*, 90–105. [CrossRef]
25. Rebhahn, J.; Stenberg Ringnér, M. World of Volvo, Gothenburg—Pushing the Boundaries. In Proceedings of the 26. Internationales Holzbau-Forum IHF, Innsbruck, Austria, 30 November–2 December 2022.
26. Acler, E. Nanyang Technological University Sports Hall—Singapore. In Proceedings of the 23. Internationales Holzbau-Forum IHF, Garmisch-Partenkirchen, Germany, 6–8 December 2017.
27. Hossain, A. Experimental Investigations of Shear Connections with Self-Tapping-Screws for Cross-Laminated-Timber Panels. Ph.D. Thesis, University of British Columbia, Vancouver, BC, Canada, 2019. [CrossRef]
28. Brown, J.; Li, M.; Tannert, T.; Moroder, D. Experimental study on orthogonal joints in cross-laminated timber with self-tapping screws installed with mixed angles. *Eng. Struct.* **2021**, *228*, 111560. [CrossRef]
29. Dietsch, P.; Ringhofer, A. Self-tapping Screws as Reinforcement for Structural Timber Elements. In *Reinforcement of Timber Elements in Existing Structures: State-of-the-Art Report of the RILEM TC 245-RTE*; Springer International Publishing: Cham, Switzerland, 2021; pp. 7–27. [CrossRef]
30. Sawata, K. Strength of bolted timber joints subjected to lateral force. *J. Wood Sci.* **2015**, *61*, 221–229. [CrossRef]
31. Dorn, M.; de Borst, K.; Eberhardsteiner, J. Experiments on dowel-type timber connections. *Eng. Struct.* **2013**, *47*, 67–80. [CrossRef]
32. Reynolds, T.; Miranda, W.; Trabucco, D.; Toumpanaki, E.; Foster, R.M.; Ramage, M.H. Stiffness and slip in multi-dowel timber connections with slotted-in steel plates. *Eng. Struct.* **2022**, *268*, 114723. [CrossRef]
33. Lemaitre, R.; Bocquet, J.F.; Schweigler, M.; Bader, T. Beam-on-Foundation Modelling as an Alternative Design Method for Timber Joints with Dowel-Type Fasteners: Part 2: Modelling Techniques for Multiple Fastener Connections. In Proceedings of the Meeting No. 6 of the International Network on Timber Engineering Research INTER, Tacoma, WA, USA, 26–29 August 2019.
34. Yurrita, M.; Cabrero, J.M. On the need of distinguishing ductile and brittle failure modes in timber connections with dowel-type fasteners. *Eng. Struct.* **2021**, *242*, 112496. [CrossRef]
35. Jorissen, A.; Fragiacomo, M. General notes on ductility in timber structures. *Eng. Struct.* **2011**, *33*, 2987–2997. [CrossRef]
36. Malo, K.; Ellingsbo, P.; Stamatopoulos, H. Notes on Deformation and Ductility Requirements in Timber Structures. In Proceedings of the Meeting No. 44 of Working Commission W18—Timber Structures, CIB-W18, Alghero, Italy, 29 August–1 September 2011.
37. Munoz, M.; Mohammad, M.; Salenikovich, A.; Quenneville, P. Need for a harmonized approach for calculations of ductility of timber assemblies. In Proceedings of the Meeting 41 of Working Commission W18—Timber Structures CIB-W18, St. Andrews, NB, Canada, 24–28 August 2008.
38. Brühl, F. Ductility in Timber Structures—Possibilities and Requirements with Regard to Dowel Type Fasteners. Ph.D. Thesis, Universität Stuttgart, Stuttgart, Germany, 2020. [CrossRef]
39. *EN 12512:2002*; Timber Structures—Test Methods—Cyclic Testing of Joints Made with Mechanical Fasteners. European Committee for Standardization CEN: Brussels, Belgium, 2002.
40. Smith, I.; Asiz, A.; Snow, M.; Chui, I. Possible Canadian/ISO approach to deriving design values from test data. In Proceedings of the Meeting 39 of Working Commission W18—Timber Structures, CIB-W18, Florence, Italy, 28–31 August 2006.
41. Jorissen, A. Double shear timber connections with dowel type fasteners. *Heron* **1999**, *44*, 163–186.
42. Jockwer, R.; Fink, G.; Köhler, J. Assessment of the failure behaviour and reliability of timber connections with multiple dowel-type fasteners. *Eng. Struct.* **2018**, *172*, 76–84. [CrossRef]

43. Gauß, J.; Kuhlmann, U. Consideration of the connection stiffness in design process—Experimental investigation. In Proceedings of the World Conference on Timber Engineering, WCTE 2018, Seoul, Republic of Korea, 20–23 August 2018; p. 7.
44. Domínguez, M.; Fueyo, J.G.; Villarino, A.; Anton, N. Structural Timber Connections with Dowel-Type Fasteners and Nut-Washer Fixings: Mechanical Characterization and Contribution to the Rope Effect. *Materials* **2022**, *15*, 242. [CrossRef] [PubMed]
45. Schweigler, M.; Bader, T.K.; Hochreiner, G.; Unger, G.; Eberhardsteiner, J. Load-to-grain angle dependence of the embedment behavior of dowel-type fasteners in laminated veneer lumber. *Constr. Build. Mater.* **2016**, *126*, 1020–1033. [CrossRef]
46. Blaß, H.J.; Schädle, P. Ductility aspects of reinforced and non-reinforced timber joints. *Eng. Struct.* **2011**, *33*, 3018–3026. [CrossRef]
47. *prEN 1995-1-1:2023*; Eurocode 5: Design of Timber Structures—Part 1-1: General Rules and Rules for Buildings. European Committee for Standardization CEN: Brussels, Belgium, 2023.
48. Blaß, H.J.; Bejtka, I.; Uibel, T. *Tragfähigkeit von Verbindungen mit Selbstbohrenden Holzschrauben mit Vollgewinde*; KIT Scientific Publishing: Karlsruhe, Germany, 2006; Volume 4.
49. González Barillas, E. Performance of Timber Connections with Single and Multiple Glued-in Threaded Steel Rods. Ph.D. Thesis, University of British Columbia, Vancouver, BC, Canada, 2015. [CrossRef]
50. Steiger, R.; Gehri, E.; Widmann, R. Glued-in steel rods: A design approach for axially loaded single rods set parallel to the grain. In Proceedings of the Meeting 37 of Working Commission W18—Timber Structures CIB-W18, Edinburgh, UK, 31 August–3 September 2004.
51. Feligioni, L.; Lavisci, P.; Duchanois, G.; De Ciechi, M.; Spinelli, P. Influence of glue rheology and joint thickness on the strength of bonded-in rods. *Holz Roh Werkst.* **2003**, *61*, 281–287. [CrossRef]
52. Parida, G.; Johnsson, H.; Fragiacomo, M. Provisions for Ductile Behavior of Timber-to-Steel Connections with Multiple Glued-In Rods. *J. Struct. Eng.* **2013**, *139*, 1468–1477. [CrossRef]
53. Gattesco, N.; Gubana, A.; Buttazzi, M. Pull-out strength of bar glued-in-joints. In Proceedings of the World Conference on Timber Engineering, WCTE 2010, Riva del Garda, Italy, 20–24 June 2010.
54. Tlustochowicz, G.; Serrano, E.; Steiger, R. State-of-the-art review on timber connections with glued-in steel rods. *Mater. Struct./Mater. Constr.* **2011**, *44*, 997–1020. [CrossRef]
55. Gehri, E. Performant Connections—A Must for Veneer-Based Products. In Proceedings of the World Conference on Timber Engineering, WCTE 2016, Vienna, Austria, 22–25 August 2016.
56. Gonzalez, E.; Avez, C.; Tannert, T. Timber Joints with Multiple Glued-in Steel Rods. *J. Struct. Eng.* **2016**, *139*, 635–651. [CrossRef]
57. Widmann, R.; Steiger, R.; Gehri, E. Pull-out strength of axially loaded steel rods bonded in glulam perpendicular to the grain. *Mater. Struct.* **2007**, *40*, 827–838. [CrossRef]
58. Fabris, A.F. Erbesserung der Zugeigenschaften von Bauholz Parallel zur Faser Mittels Verbund mit Profilierten Stahlstangen. Ph.D. Thesis, ETH Zurich, Zurich, Switzerland, 2001. [CrossRef]
59. Otero Chans, D.; Estévez Cimadevila, J.; Martín Gutiérrez, E. Orientation of bars glued on glued laminated products: Parallel vs. perpendicular. *Compos. Part B Eng.* **2014**, *62*, 97–103. [CrossRef]
60. Blaß, H.J.; Laskewitz, B. *Glued-in Rods for Timber Structures: Effect of Distance between Rods and between Rods and Timber Edge on the Axial Strength*; Versuchsanstalt für Stahl, Holz und Steine, Abt. Ingenieurholzbau: Karlsruhe, Germany, 2001.
61. Jockwer, R.; Steiger, R.; Frangi, A. Fully Threaded Self-tapping Screws Subjected to Combined Axial and Lateral Loading with Different Load to Grain Angles. In Proceedings of the Materials and Joints in Timber Structures, Stuttgart, Germany, 8–10 October 2013; Aicher, S., Reinhardt, H.W., Garrecht, H., Eds.; Springer: Dordrecht, The Netherlands, 2014; pp. 265–272.
62. Tomasi, R.; Crosatti, A.; Piazza, M. Theoretical and experimental analysis of timber-to-timber joints connected with inclined screws. *Constr. Build. Mater.* **2010**, *24*, 1560–1571. [CrossRef]
63. *EN 26891:1991*; Timber Structures—Joints Made with Mechanical Fasteners—General Principles for the Determination of Strength and Deformation Characteristics. European Committee for Standardization CEN: Brussels, Belgium, 1991.
64. Martin, W.T.; Spanier, E.H.; Springer, G.; Davis, P.J. *Principle of Mathematical Analysis*; McGraw-Hill, Inc.: New York, NY, USA, 1963.
65. Cabrero, J.M.; Honfi, D.; Jockwer, R.; Yurrita, M. A probabilistic study of brittle failure in dowel-type timber connections with steel plates loaded parallel to the grain. *Wood Mater. Sci. Eng.* **2019**, *14*, 298–311. [CrossRef]